International Journal of Minerals, Metallurgy and Materials
Volume 26, Number 4, April 2019, Page 523
https://doi.org/10.1007/s12613-019-1760-6

A study of interparticulate strain in a hot-extruded SiC_p/2014 Al composite

Ying Hu[1,2], *Qiu-bao Ou-yang*[1,3], *Lei Yao*[2], *Sheng Chen*[2], *and Lan-ting Zhang*[1,4]

1) School of Materials Science and Engineering, Shanghai Jiao Tong University, Shanghai 200240, China
2) Support Department of Research Institute (R&D Center), Baoshan Iron & Steel Co., Ltd., Shanghai 201900, China
3) State Key Laboratory of Metal Matrix Composites, Shanghai Jiao Tong University, Shanghai 200240, China
4) Materials Genome Initiative Center, Shanghai Jiao Tong University, Shanghai 200240, China
(Received: 19 June 2018; revised: 14 October 2018; accepted: 19 October 2018)

Abstract: We report a correlative study of strain distribution and grain structure in the Al matrix of a hot-extruded SiC particulate-reinforced Al composite (SiC_p/2014 Al). Finite element method (FEM) simulation and microstructure characterization indicate that the grain structure of the Al matrix is affected by the interparticulate strain distribution in the matrix during the process. Both electron-backscattered diffraction (EBSD) and selected-area electron diffraction (SAED) indicated localized misorientation in the Al matrix after hot extrusion. Scanning transmission electron microscopy (STEM) revealed fine and recrystallized grains adjacent to the SiC particulate and elongated grains between the particulates. This result is explained in terms of recrystallization under an interparticulate strain distribution during the hot extrusion process.

Keywords: metal-matrix composites; strain distribution; recrystallization; grain structure

1. Introduction

Hot extrusion is usually used to prepare Al–SiC particulate-reinforced composites by either the ingot or powder metallurgy route [1–2]. In the hot extrusion process, SiC_p/Al composites undergo a certain degree of plastic deformation depending on the extrusion ratio. Because SiC is a hard particulate, the plastic deformation is accommodated by deformation of the Al matrix, which results in strain in the metal matrix [3–4]. During the hot extrusion, recrystallization occurs simultaneously, which gives rise to a complicated microstructure evolution that includes residual strain and the grain structure in the composite [5–6]. Understanding the aforementioned microstructural evolution is important in optimizing the processing parameters for balanced properties in applications [7–11].

The chemical composition of the 2014 Al alloy is shown in Table 1. The SiC particles used in this study are α-SiC with an average particle size of 10 μm. The 2014 Al alloy with 14wt% SiC particle reinforced composite ingots were prepared via the stir-casting route followed by hot extrusion with an extrusion ratio of 4:1 in area. During the extrusion, the billet was heated to 450–470°C and subjected to molding at a pressing force of 60 MN and an extrusion speed of 2 m/min. The average grain size of the aluminum matrix in the as-cast state was 100–230 μm, and after extrusion it was 5 μm. The processing temperature was well above the recrystallization initiation temperature of Al, which is usually 320°C [12].

Table 1. Chemical composition of 2014 Al alloy wt%

Cu	Si	Mn	Fe	Mg	Ni	Zn	Ti	Al
3.9–4.8	0.5–1.2	0.4–1.0	≤ 0.7	0.4–0.8	≤ 0.10	≤ 0.30	≤ 0.15	Balance

Fathy and other researchers indicated that the processing route [13–17] and the grain size of the reinforcement phase [18–20] strongly affect composite properties [21–22]. To ensure reliable results, the same batch of SiC particles

Corresponding author: Lan-ting Zhang E-mail: lantingzh@sjtu.edu.cn

was selected and the process parameters were kept stable during the experiments in the present work.

The focus of this paper is on understanding the interparticulate strain distribution in the Al matrix and the resulting recrystallization during processing by both finite element simulation and microstructure characterization. First, we assumed that the microstructure of the material was stable during the heat treatment and then calculated the interparticulate strain distribution of the Al matrix by the finite element method (FEM), especially the strain between the two SiC particulates. Then, the strain in the SiC_p/Al composites was characterized by electron-backscattered diffraction (EBSD) and compared with the calculation results. Details of the interparticulate grain structure in the metal matrix were studied by scanning transmission electron microscopy (STEM), and the results were correlated with the effects of the strain on the recrystallization of Al matrix during hot extrusion of the SiC_p/Al composites.

2. FEM modeling and simulation

A commercial FEM code, DEFORM 2D ver 9.0, was used to carry out the simulation of the hot extrusion process. Fig. 1(a) is a schematic of the hot extrusion process with an

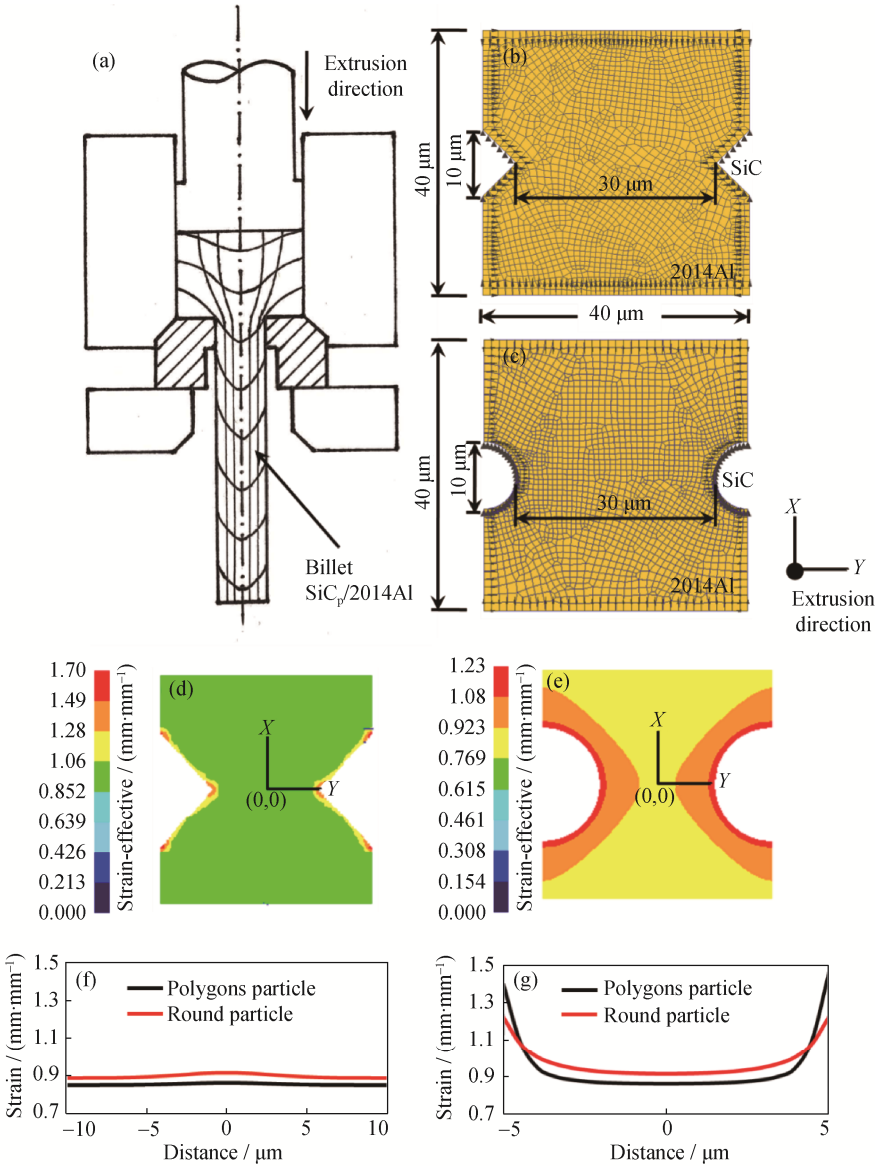

Fig. 1. Simulation of the hot extrusion: (a) schematic of the hot extrusion process (extrusion direction is indicated by the arrow); model and constraint conditions in the billet core with polygons SiC particles (b) and round SiC particles (c) along the cross section (the yellow region is 2014 Al); distribution of strain in the composite at the end of simulation with polygons SiC particles (d) and round SiC particles (e); strain distribution along the *X* direction (f) and *Y* direction (g) between two SiC particulates.

extrusion ratio of 4:1 in area. To capture the strain distribution between the two SiC particulates during hot extrusion, a 2D model measuring 40 μm × 40 μm along the cross section of the billet was established (vertical to the extrusion direction (Figs. 1(b) and 1(c)), where the two SiC particulates were placed on the two opposite sides of the model. Both 10-μm polygons (Fig. 1(b)) and round (Fig. 1(c)) SiC particulates were considered in the model to simulate the polyhedral and nearly spherical particulates used in the composite. The initial spacing between the two SiC particulates was set to 30 μm and was reduced to 10 μm after extrusion. This spacing corresponds to a reduction in cross section from 1600 μm^2 to 400 μm^2 during extrusion and to the observed average SiC spacing in the microstructure. The relative position of the SiC particles was assumed to remain unchanged during the extrusion process, i.e., at the center of the side boundary of the model. Meanwhile, because the model captured only the central part of the cross section during extrusion, no dead zone at the edge or end of the mold was involved and the position of the two particles was not affected by the dead zone.

For the sake of simplicity, both the die and SiC particles were considered to be rigid and no recrystallization occurred in the 2014 Al matrix. The plane strain boundary condition was applied to the four edges of the 2D model. The SI unit system was selected at the beginning of the simulation, and parameters for commercial 2014 Al from the DEFORM material database were adopted. Friction between the SiC particulates and the 2014 Al matrix was not considered, and the heating due to fiction was ignored. The 2014 Al matrix was divided into 2,000 four-node quadrilateral elements that were automatically re-meshed if they became too distorted during the simulation process [23–25]. The extrusion simulation was performed at 450°C under a nominal rate of 2 m/min and 60 MN force. The reduction in cross section from 1600 μm^2 to 400 μm^2 was divided into 50 steps during simulation.

Figs. 1(d) and 1(e) show the strain distribution at the end of hot extraction in the two models, where the strain distribution is heavily localized at the tips of the polygonal SiC particulate, whereas it is rather uniform along the edge of round SiC particulate. Figs. 1(f) and 1(g) are the strain (Positive value indicates compressive in the model) distribution in *x* and *y* directions in the 2014 Al matrix after hot extrusion. In the *x* direction, a rather constant strain distribution is observed (Fig. 1(f)). However, obvious strain concentration in the vicinity of the SiC particulate is observed between the two SiC particulates in the *y* direction (Fig. 1(g)). Because no recrystallization of the Al matrix is considered, the strain in the simulation is relatively high. The strain at the tip of the polyhedral SiC particulate is much larger than that at the frontier of the nearly spherical particulate. The strain decreases sharply with increasing distance from the SiC particulate. In the platform part of the strain distribution in both *x* and *y* directions, the strain is slightly higher for the nearly spherical particle case than for the polyhedron counterpart. The simulation clearly indicates that the SiC particulate with a sharp corner generates a relatively high strain in the Al matrix near the particulate during hot extrusion.

3. Microstructure characterization of SiCp/Al composites

3.1. Characterization methods and sample preparation

EBSD (OXFORD Instruments) and transmission electron microscopy (TEM, JEOL JEM-2100) were used to study the microstructure and strain of the as-extruded SiC_p/Al composite. STEM (JEOL JEM-2100F) was used to observe the grain structure of the 2014 Al matrix.

Figs. 2(a) and 2(b) are the optical morphology of a composite before and after extrusion, respectively. The SiC clusters into a colony in the as-cast state and is uniformly distributed in the Al matrix after extraction. Special care was taken in sample preparation for EBSD analysis because of the large difference in physical and chemical properties of the SiC particulates and the 2014 Al matrix. To ensure the desired surface roughness of the SiC_p/2014 Al composite for EBSD analysis, samples were prepared by Ar-ion cross-sectional polishing (CP, JEOL SM09020) under an accelerating voltage of 5 kV and a beam current of 0.1 mA for 10 h. An observation area larger than 0.5 mm × 1.5 mm could be prepared. Fig. 2(d) shows the surface roughness of the samples prepared by mechanical grinding and CP. In the mechanically ground sample, the height difference between the SiC particulate and Al matrix measured by confocal scanning optical microscopy (dark line in Fig. 2(b)) was at the micrometer level. In contrast, the height difference in the CPed sample was imaged in topological mode using an electron-probe microanalyzer (EPMA-TOPO, JEOL 8500F) (Fig. 2(c)). Measurement by atomic force microscopy (AFM, Molecular Imaging Pico Scan 2500) showed that it was at the nanometer scale (Fig. 2(d)).To observe the microstructure at the SiC_p/2014 Al interface region by TEM, site-specific samples were prepared by the focused-ion-beam technique (FIB, SII SMI 3050). The thickness of the sample was approximately 60 nm.

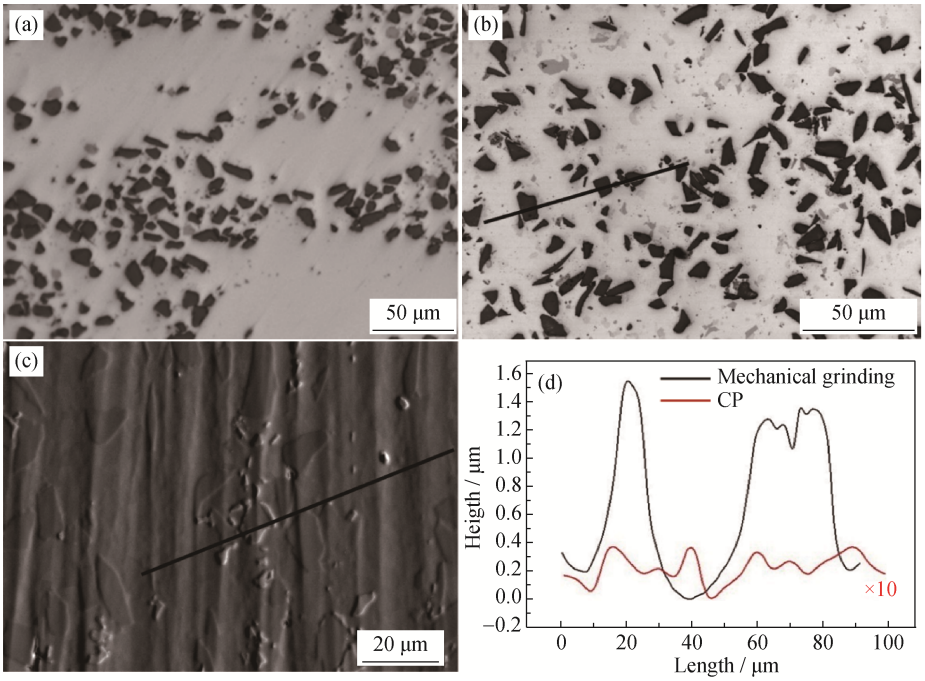

Fig. 2. Morphology and surface roughness of SiC_p/2014 Al: (a) optical image of as-cast SiC_p/2014 Al; (b) confocal scanning optical image of hot-extruded SiC_p/2014 Al prepared by mechanical grinding; (c) back-scattered image of a cross-section of polished (CPed) SiC_p/2014 Al in topological mode (EPMA-TOPO); (d) comparison of the surface roughness across the line in the corresponding images ((b) & (c)) for the two samples (the data for the CPed sample are multiplied by 10 for clarity).

3.2. EBSD characterization of the SiC_p/Al composite

A local misorientation map generated by EBSD can be used to characterize the strain in the 2014 Al matrix of the composite [26]. Local misorientation is defined as the average lattice orientation difference between each point and its eight neighbors. Misorientations greater than 5° are regarded as grain boundaries [27]. Fig. 3(a) is a low-magnification local misorientation map of the as-extruded SiC_p/2014 Al composite perpendicular to the extrusion direction, where some localized regions of misorientation in green stripes are clearly observed in the 2014 Al matrix. This observation indicates an inhomogeneous distribution of strain in the composite after extrusion. The grains of the 2014 Al matrix are equiaxed, showing a size distribution of ~3.0 ± 1.3 μm. Fig. 3(b) shows a high-magnification image of the local misorientation distribution in the grains around a SiC particulate in the as-extruded composite. According to the color scale [28], the local misorientation is unevenly distributed: some grains show a higher extent of strain accumulation than others do. This uneven deformation of grains is reasonable because the crystal orientation of each grain is different. However, because of the resolution limit of EBSD, details of the region near the SiC particulate are not shown.

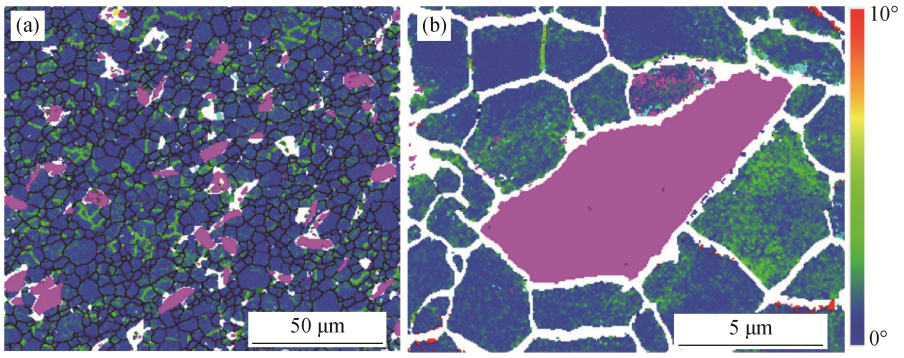

Fig. 3. Local misorientation map: (a) grain boundary and misorientation map of a hot-extruded SiC_p/2014 Al; (b) the misorientation map around SiC. Black lines in (a) are grain boundaries, $\theta > 5°$; Rainbow scales in (a) and (b): pink represents SiC; blue represents 0° misorientation from reference; red represents 10° misorientation from reference.

3.3. TEM/STEM characterization of as-extruded SiC_p/Al composite

The bright-field TEM image shows a strong strain contrast fringe in the 2014 Al matrix similar to that reported in [29], where individual grains cannot be observed (Fig. 4(a)). The [011]-zone SAED pattern clearly indicates a lattice rotation around the zone axis between 2° and 5° (Fig. 4(b)), where the measured rotation of the diffraction spot is consistent with the local misorientation observed by EBSD. No particular strain contrast is observed in the SiC particulate. Details of the grain structure neighboring the SiC particulate is revealed by a bright-field STEM image (Fig. 5(a)), where the strain contrast plays a minor role. The dark dots are fine $CuAl_2$ precipitates. As sketched in Fig. 5(b), two types of Al grains neighbor the SiC particulate: those directly adjacent to the SiC are equiaxed grains of submicron scale (~0.2 μm), and those in the outer region are elongated grains ~1 μm in the longitude direction. The thickness of the equiaxed grains zone is 2–3 μm around the SiC particulate.

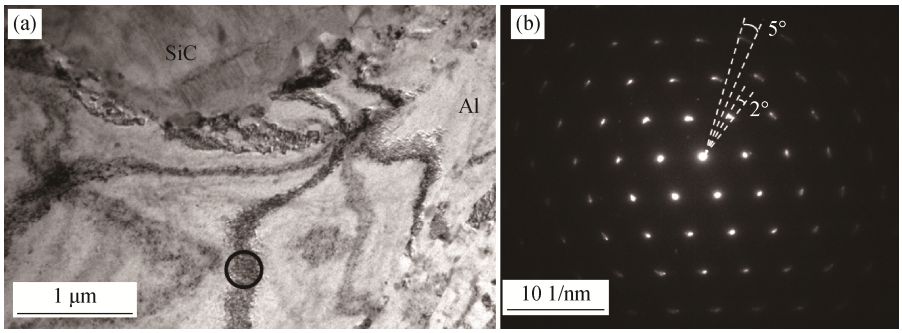

Fig. 4. (a) Bright-field TEM image of SiC_p/2014 Al showing strong strain contrast in the Al matrix; (b) SAED pattern of the circled region in (a), showing a crystal rotation of approximately 2°–5°.

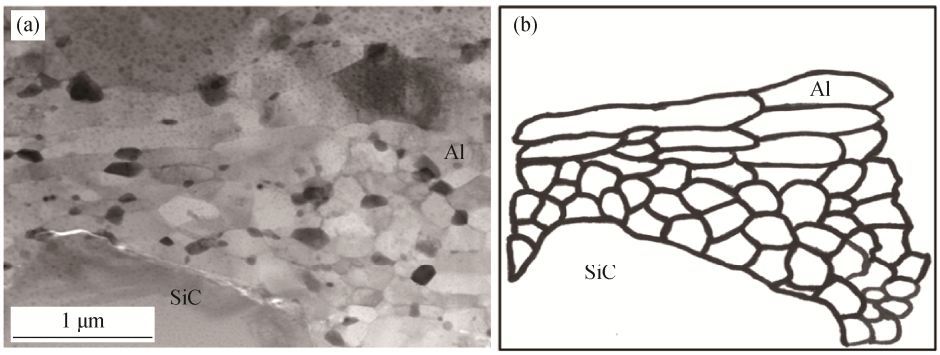

Fig. 5. (a) Bright-field STEM image of SiC_p/2014 Al showing grains of the Al matrix at the SiC_p/Al interface (the dark dots are $CuAl_2$); (b) schematic of the grains between the SiC particles in (a).

4. Discussion

Because the processing temperature (450–470°C) is well above the recrystallization initiation temperature of Al (320°C), both deformation and recrystallization occur in the Al matrix during the hot extrusion. Even though the FEM simulation indicates rather high and uniform strain in the Al matrix between the SiC particulates (Figs. 1(d) and 1(e)), experimental observations show rather limited residual strain in the Al matrix and equiaxed grains of Al in general. The mean size of the Al grains is ~3.0 μm and exhibits a Gaussian distribution. These results indicate that recrystallization in the Al matrix during hot extrusion even though it is not accounted for in the FEM simulation [30].

In the area adjacent to the SiC particulate, the FEM simulation indicates a rather high strain and quickly decreases as a function of distance from the particulate (Fig. 1(e)). This region is estimated to be ~1 μm. Within this region, the STEM image indicates much finer grain size than those away from the particulate (Fig. 5). This result is consistent with the high strain predicted by the FEM simulation. The recrystallization nucleation rate C can be described by the Arrhenius equation as follows:

$$C = C_0 \mathrm{e}^{-\frac{Q}{RT}} \tag{1}$$

where Q is the recrystallization nucleation activation energy; R is a gas constant; T is the absolute temperature; and C_0 is a proportional constant. According to a previous study [31],

the recrystallization nucleation activation energy can be decreased by a large deformation. However, recrystallization and growth during extrusion is strongly affected by both thermodynamics and kinetics, especially under an excessive extrusion speed of 2 m/min. Even though both the Al matrix near and far from the SiC particulate tends to recrystallize, the kinetics only allows the grains close to the SiC particulate to recrystallize fully under the present extrusion process. Thus, the nucleation rate close to the SiC particulate is high because of the large strain leading to a much finer grain than those far from the particulate. Moreover, the thickness of the fine grain region around the SiC particulate (Fig. 5(a)) roughly agrees with the length of the rapid decrease region of strain in the simulation (Fig. 1(g)).

5. Conclusions

The results of the present work show that plastic deformation and recrystallization in the 2014 Al matrix occur simultaneously during the hot extrusion process. Strain accumulates obviously adjacent to the SiC particulates and decreases quickly with increasing distance. A platform region of strain distribution is found between the SiC particulates. The uneven distribution of strain gives rise to different recrystallization behavior of the metal matrix during hot extrusion. Understanding the evolution of grain structure during hot extrusion offers an opportunity to optimize the hot extrusion process parameter and thus improve the desired properties.

Acknowledgement

This work is financially supported by the National Basic Research Program of China (973) (No. 2012CB619600).

References

[1] S.S. Li, Y.S. Su, Q.B. Ouyang, and D. Zhang, *In-situ* carbon nanotube-covered silicon carbide particle reinforced aluminum matrix composites fabricated by powder metallurgy, *Mater. Lett.*, 167(2016), p. 118.

[2] J.M. Root, D.P. Field, and T.W. Nelson, Crystallographic texture in the friction-stir-welded metal matrix composite Al6061 with 10 vol pct Al_2O_3, *Metall. Mater. Trans. A*, 40(2009), No. 9, p. 2109.

[3] S.J. Hong, H.M. Kim, D. Huh, C. Suryanarayana, and B.S. Chun, Effect of clustering on the mechanical properties of SiC particulate-reinforced aluminum alloy 2024 metal matrix composites, *Mater. Sci. Eng.*, *A*, 347(2003), No. 1-2, p. 198.

[4] Z. Xue, Y. Huang, and M. Li, Particle size effect in metallic materials: A study by the theory of mechanism-based strain gradient plasticity, *Acta Mater.*, 50(2002), No. 1, p. 149.

[5] D. Mandal and S. Viswanathan, Effect of re-melting on particle distribution and interface formation in SiC reinforced 2124Al matrix composite, *Mater. Charact.*, 86(2013), p. 21.

[6] D. Mandal and S. Viswanathan, Effect of heat treatment on microstructure and interface of SiC particle reinforced 2124 Al matrix composite, *Mater. Charact.*, 85(2013), p. 73.

[7] G. Liu, G.J. Zhang, R.H. Wang, W. Hu, J. Sun, and K.H. Chen, Heat treatment-modulated coupling effect of multi-scale second-phase particles on the ductile fracture of aged aluminum alloys, *Acta Mater.*, 55(2007), No. 1, p. 273.

[8] R. Vogt, Z. Zhang, Y. Li, M. Bonds, N.D. Browning, E.J. Lavernia, and J.M. Schoenung, The absence of thermal expansion mismatch strengthening in nanostructured metal-matrix composites, *Scripta Mater.*, 61(2009), No. 11, p. 1052.

[9] J.S. Robinson and W. Redington, The influence of alloy composition on residual stresses in heat treated aluminium alloys, *Mater. Charact.*, 105(2015), p. 47.

[10] J.Y. Song, Q. Guo, Q.B. Ouyang, Y.S. Su, J. Zhang, E.J. Lavernia, J.M. Schoenung, and D. Zhang, Influence of interfaces on the mechanical behavior of SiC particulate-reinforced Al–Zn–Mg–Cu composites, *Mater. Sci. Eng. A*, 644(2015), p. 79.

[11] Z.Z. Chen, Z.Q. Tan, G. Ji, G.L. Fan, D. Schryvers, Q.B. Ouyang, and Z.Q. Li, Effect of interface evolution on thermal conductivity of vacuum hot pressed SiC/Al composites, *Adv. Eng. Mater.*, 17(2015), No. 7, p. 1077.

[12] S.Y. Wang, Q. Tang, D.J. Li, J.X. Zou, X.Q. Zeng, Q.B. Ouyang, and W.J. Ding, The hot workability of SiC_p/2024 Al composite by stir casting, *Mater. Manuf. Processes*, 30(2015), No. 5, p. 624.

[13] A. Fathy, D. Ibrahim, O. Elkady, and M.Hassan, Evaluation of mechanical properties of 1050-Al reinforced with SiC particles via accumulative roll bonding process, *J. Compos. Mater.*, 53(2019), No. 2, p. 209.

[14] N.E. Mahallawy, A. Fathy, and M. Hassan, Evaluation of mechanical properties and microstructure of Al/Al–12%Si multilayer via warm accumulative roll bonding process, *J. Compos. Mater.*, 2017. https://doi.org/10.1177/0021998317692141

[15] N.E. Mahallawy, A. Fathy, W. Abdelaziem, and M. Hassan, Microstructure evolution and mechanical properties of Al/Al–12%Si multilayer processed by accumulative roll bonding (ARB), *Mater. Sci. Eng.*, *A*, 647(2015), p. 127.

[16] A. Fathy, O. Elkady, and A. Abu-Oqail, Synthesis and characterization of Cu–ZrO_2 nanocomposite produced by thermochemical process, *J. Alloys Compd.*, 719(2017), p. 411.

[17] A. Fathy, Investigation on microstructure and properties of Cu–ZrO_2 nanocomposites synthesized by in situ processing, *Mater. Lett.*, 213(2018), p. 95.

[18] A. Fathy, A. Sadoun, and M. Abdelhameed, Effect of matrix/reinforcement particle size ratio (PSR) on the mechanical properties of extruded Al–SiC composites, *Int. J. Adv. Manuf. Technol.*, 73(2014), No. 5-8, p. 1049.

[19] O. El-Kady and A. Fathy, Effect of SiC particle size on the physical and mechanical properties of extruded Al matrix nanocomposites, *Mater. Des.*, 54(2014), p. 348.

[20] A. Wagih, A. Fathy, D. Ibrahim, O. Elkady, and M. Hassan, Experimental investigation on strengthening mechanisms in Al–SiC nanocomposites and 3D FE simulation of Vickers indentation, *J. Alloys Compd.*, 752(2018), p. 137.

[21] A. Wagih and A. Fathy, Improving compressibility and thermal properties of Al–Al_2O_3 nanocomposites using Mg particles, *J. Mater. Sci.*, 53(2018), No. 16, p. 11393.

[22] A. Fathy and O. El-Kady, Thermal expansion and thermal conductivity characteristics of Cu–Al_2O_3 nanocomposites, *Mater. Des.*, 46(2013), p. 355.

[23] J. Zhang, Q.B. Ouyang, Q. Guo, Z.Q. Li, G.L. Fan, Y.S Su, L. Jiang, E.J. Lavernia, J.M. Schoenung, and D. Zhang, 3D microstructure-based finite element modeling of deformation and fracture of SiC_p/Al composites, *Compos. Sci. Technol.*, 123(2016), p. 1.

[24] H. Jiang, Z.G. Fan, and C.Y. Xie, 3D finite element simulation of deformation behavior of CP-Ti and working load during multi-pass equal channel angular extrusion, *Mater. Sci. Eng. A*, 485(2008), No. 1-2, p. 409.

[25] H. Jiang, Z.G. Fan, and C.Y. Xie, Finite element analysis of temperature rise in CP-Ti during equal channel angular extrusion, *Mater. Sci. Eng. A*, 513–514(2009), p. 109.

[26] V. Ocelík, J.A. Vreeling, and J.T.M. De Hosson, EBSP study of reaction zone in SiC/Al metal matrix composite prepared by laser melt injection, *J. Mater. Sci.*, 36(2001), No. 20, p. 4845.

[27] M. Kamaya, Assessment of local deformation using EBSD: Quantification of local damage at grain boundaries, *Mater. Charact*., 66(2012), p. 56.

[28] J. Guo, S. Amira, P. Gougeon, and X.G. Chen, Effect of the surface preparation techniques on the EBSD analysis of a friction stir welded AA1100-B_4C metal matrix composite, *Mater. Charact.*, 62(2011), No. 9, p. 865.

[29] Z.P. Luo, Y.G. Song, and S.Q. Zhang, A TEM study of the microstructure of SiC_p/Al composite prepared by pressure less infiltration method, *Scripta Mater.*, 45(2001), No. 10, p. 1183.

[30] W.L Zhang, J.X. Wang, F. Yang, Z.Q. Sun, and M.Y. Gu, Recrystallization kinetics of cold-rolled squeeze-cast Al/SiC/15w composites, *J. Compos. Mater.*, 40(2006), No. 12, p. 1117.

[31] F.J. Humphreys and M. Hatherly, *Recrystallization and Related Annealing Phenomena*, Pergamon Press, Oxford, 2004, p. 451.